IEEE Access
Multidisciplinary | Rapid Review | Open Access Journal

Received May 12, 2020, accepted May 25, 2020, date of publication June 8, 2020, date of current version June 18, 2020.

Digital Object Identifier 10.1109/ACCESS.2020.3000581

Rat Head Phantom for Testing of Electroencephalogram Source Localization Techniques

JAROSLAV LACIK[1], (Member, IEEE), VLASTIMIL KOUDELKA[2], DAVID KURATKO[1], ZBYNEK RAIDA[1], (Senior Member, IEEE), DANIEL KRZYSZTOF WÓJCIK[1,3], TOMAS MIKULASEK[1], JIRI VANEK[4], STANISLAV JIRICEK[2,5], AND CESTMIR VEJMOLA[2]

[1]Department of Radio Electronics, Faculty of Electrical Engineering and Communication, Brno University of Technology, 616 00 Brno, Czech Republic
[2]National Institute of Mental Health, 250 67 Klecany, Czech Republic
[3]Nencki Institute of Experimental Biology, Polish Academy of Sciences, 02-093 Warsaw, Poland
[4]Department of Electrical and Electronics Technology, Faculty of Electrical Engineering and Communication, Brno University of Technology, 616 00 Brno, Czech Republic
[5]Department of Cybernetics, Faculty of Electrical Engineering, Czech Technical University in Prague, 121 35 Prague, Czech Republic

Corresponding author: Jaroslav Lacik (lacik@feec.vutbr.cz)

This work was supported by the Czech Science Foundation under Grant 18-16218S.

ABSTRACT In this paper we report a new rat head phantom developed for testing electroencephalogram source localization techniques. The phantom is composed of an agar based mixture mimicking the rat brain, six dipoles and fourteen electrodes for modeling and monitoring of neural activity of the brain, respectively, and a 3D printed skull based on a computed tomography scan of a rat skull. In order to fabricate the phantom with currently available conventional techniques, the phantom is 1.8 times enlarged. To allow scaling, we performed an extensive study of electric properties of the agar based mixture, including electric conductivity, permittivity, and applied voltage, to ensure a linear operating regime. The new phantom facilitates testing of existing and the development of new cortical electrode implants as well as studying the quality of various source localization techniques.

INDEX TERMS Rat head phantom, electroencephalogram source localization, complex permittivity measurement, agar, 3D printing.

I. INTRODUCTION

The goal of electroencephalogram (EEG) source localization is finding positions of EEG wave sources located inside the brain. In other words, electric activity inside the rat's brain volume is estimated from EEG signals measured on the rat brain surface. Generally, two problems are considered in the context of source localization. The first problem, called the forward problem, evaluates the potential at the brain surface for known positions of electric sources located inside the brain [1]. To model neural activity of the brain in the context of EEG, electric current dipoles defined by their dipole moment are usually used. The second problem, called the inverse problem, exploits the relations established in the forward model to identify the distribution of brain sources from the potentials measured on the head surface. For validation of appropriate solving of both problems, adequate phantoms are useful [2]–[10].

Head phantoms can be digital or physical. In digital phantoms [2]–[5], it is relatively easy to take into account the shape, composition and electric/magnetic properties of the head, as well as to include the neural activity in the brain. Unfortunately, it is more difficult to take into account motion artifacts, realistic electromagnetic interference (EMI), and to test the EEG measurement system. Physical phantoms have not been able to mimic reality as the digital ones have, however, mainly due to the development of modern technology in recent years, e.g. 3D printing, their credibility from the viewpoint of reality modeling have grown significantly. Note that physical phantoms do not carry the above-mentioned disadvantages of digital phantoms.

Various physical phantoms have been created. They include a saline filled tank [6], a human skull phantom [7], mold phantoms based on conductive materials [8], gelatin

The associate editor coordinating the review of this manuscript and approving it for publication was Larbi Boubchir.

This work is licensed under a Creative Commons Attribution 4.0 License. For more information, see https://creativecommons.org/licenses/by/4.0/

phantoms [9], [5] and 3D printed phantoms [10] which are also able to mimic anisotropy of head tissues. A common feature of all those phantoms, apart from [9] which is a simple gelatin block phantom, is the fact that they all mimic the human head. We are not aware of any rat head phantom available for testing EEG equipment or techniques. Although the techniques for the creation of the rat head phantom are similar as for the human one, we can see several differences which have to be considered:

- The shape and size of heads are significantly different. To fabricate a rat head phantom with conventionally available techniques, the size of the phantom has to be scaled (increased) which imposes stress on the linear behaviour of the phantom. Scaling of the phantom allows us to also minimize the influence of the excitation dipoles and the feeding part on the measured potentials.
- The EEG monitoring of a human brain is noninvasive, whereas the monitoring of a rat is usually invasive. Thus, the electrodes for monitoring the neural activity of a rat brain have to be included in the phantom.

The source localization problem belongs to a class of so called ill-posed problems. Generally, a small perturbation in any of the above-mentioned steps can lead to high error in source reconstruction. To achieve reliable source reconstructions, uncertainties in all of the steps have to be treated carefully [11].

Recently, source localization in rodents has been investigated for preclinical and translational research [12], [13]. Various techniques have been used for EEG acquisition: high density scalp EEG cap [12], [14], skull EEG microarray [15], and regular cortical electrode array [13]. Scalp and scull electrode systems were tested in vivo on a limited set of brain activations. The cortical electrode system was validated on a block shaped phantom in [9].

The current study focuses on validating source localization techniques in rats. The aim of this study is to develop a model for testing various inverse solvers and implants. The rat preclinical models are essential for modelling various brain diseases and effects of drugs with respect to their clinical potential. Developing source localization techniques and validation methods in rats is essential for transitioning from the preclinical rat model to a human. To the best of our knowledge, no standardized and validated solutions of the inverse localization in rats have been established so far.

Our goal was to fabricate a realistically shaped phantom containing an original cortical electrode system used in our previous preclinical studies [16]. The implant containing twelve sensing electrodes touching the brain surface, one reference electrode located above the olfactory bulb, and one grounded electrode placed subcutaneously in the occipital part of the head, was originally designed to acquire signals from known functional areas of the rat brain. Thus, the electrode positions were not originally optimized for source localization techniques. The design of the phantom in this work corresponds to our current electrode system. The presented technique of phantom fabrication and the phantom itself serves as one of the tools for evaluating source localization techniques in the future development of the electrode system.

The organization of the paper is the following. Section II deals with a deep investigation of the agar based mixture for mimicking the rat brain. Section III shortly describes excitation dipoles and electrodes for modeling and monitoring of the neural activity of the brain. Sections IV and V deals with the rat head phantom fabrication and testing, respectively. Section VI concludes the paper.

II. HOMOGENEOUS BRAIN EQUIVALENT

At this stage of the phantom development, our aim is to model the brain by a homogeneous medium with dielectric properties close to gray matter since most neural activity is concentrated there.

Dielectric properties of brain tissues depend on many factors such as animal age or ambient temperature. In addition, obtained parameter values may also depend on the type of measuring method. Most of the researchers focus mainly on the characterization of brain tissues by their electrical conductivity, which may be frequency-dependent. Further, note that brain tissue is anisotropic. For example, the conductivity of the white matter is much more directional than that of the gray matter [17]–[19].

Although the conductivity of the gray matter cannot be described by one number, the problem is now simplified by approximating the conductivity of the used homogeneous phantom to 0.33 S/m which is a widely used value of gray matter conductivity in EEG forward problem modeling [3].

A. TUNING AGAR BASED MIXTURE

Our homogeneous equivalent brain is based on a mixture of deionized water, sodium chloride (NaCl) and agar [20], [5]. Although agar based phantoms lack a low time span due to water evaporation and possible fungi growing, their fabrication is easy and no special equipment is necessary.

Deionized water is used as the main constituent of the mixture since water is the foundation of biological tissues. NaCl is used to control electrical conductivity and agar is used for solidifying the mixture.

In [20], extensive investigation was carried out to describe the dependence of the electrical conductivity of the agar based mixtures on NaCl doping

$$\sigma = 215 \cdot c + 0.0529. \tag{1}$$

Here σ and c are the agar based mixture conductivity (S/m) and NaCl concentration (g/ml), respectively. In [5], authors reported that the measured conductivity of fabricated agar samples were different than predicted by (1). This inconsistency could be caused by using different agar powders in [20] and [5]. So in [5], different mixtures over various NaCl concentrations were measured and the following modified linear regression model was proposed

$$\sigma = 179 \cdot c + 0.032. \tag{2}$$

Evidently, the electrical conductivity of the agar based mixtures depends on quality/purity of used constituents and has to be measured on samples fabricated from used constituents. Unfortunately, the published values of electrical conductivity of agar mixtures lack information about voltage applied on measured samples. That information is critical from the viewpoint of linearity. Further, the open literature contains no information about what the agar based mixture permittivity is, and how it varies with frequency. The displacement current is critically influenced by the established permittivity value.

Those issues forced us to investigate agar based mixtures in more detail. For the study, we used deionized water from Sigma-Aldrich, an extra pure agar powder from Himedia, and NaCl from PENTA.

Various mixtures of deionized water, agar and NaCl were fabricated in the following way: the NaCl solution was stirred at room temperature of 23°C with a magnetic stirring bar for 10 minutes. After that, the solution was continuously stirred and heated to 80°, which took about 12 minutes. Then the agar powder was added and melted in the solution. After 4 minutes the temperature of the mixture was about 85°C. The solution was poured into the cube-shaped mold with side dimensions of 30 mm and cooled to room temperature for solidification.

The base and the side walls of the mold were printed by a 3D printer based on fused deposit manufacturing (FDM) and using a polylactic (PLA) filament. The front and the back of the mold were realized by platinum plated electrodes. So the mold was also a sample holder. To measure the electrical properties of the mixture, the holder was connected to a precision LCR meter Agilent 4284A by a 4-point clip test set to minimize the transitional impedance (Fig. 1). The measurement was carried out in the frequency range from 20 Hz to 50 kHz.

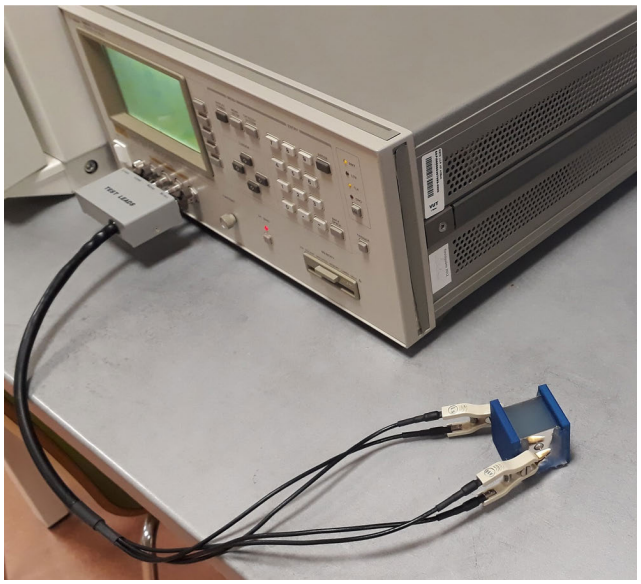

FIGURE 1. Measurement setup for agar based mixture characterization.

From the measured conductivity G and the capacitance C, the electrical conductivity

$$\sigma = \frac{Gt}{A}, \tag{3}$$

and relative permittivity

$$\varepsilon_r = \frac{Ct}{\varepsilon_0 A} \tag{4}$$

of the mixture can be determined [21]. Here, t is the thickness of the sample, A is the area of electrodes, and ε_0 is the permittivity of the vacuum.

After several iterations, we found that our homogeneous brain equivalent with the target value of the electric conductivity of 0.33 S/m can be approximated by the following final mixture composition: deionized water 199.72 g, NaCl 0.28 g, and agar 4 g. That composition was considered to be the reference one, and we further measured other mixtures with different doping of NaCl. However, the total mass and the amount of agar were the same. The measured mixtures are summarized in Table 1. Mixture no. 3 represents the final composition for the homogeneous brain equivalent.

TABLE 1. Composition of investigated mixtures.

Mixture no.	Deionized water (g)	NaCl (g)	Agar (g)
1	200.00	0.00	4.00
2	199.86	0.14	4.00
3	199.72	0.28	4.00
4	199.44	0.56	4.00
5	198.88	1.12	4.00

The measured frequency response of electrical conductivity and relative permittivity of investigated mixtures are depicted in Fig. 2. Note that the voltage level of the LCR meter oscillator was set to 1 V (the effective value – root mean square value – of the sine wave which corresponds to the amplitude of 1.41 V) for all the measurements. Obviously, both electrical values depend on the measuring frequency values. The frequency dependence of the electric conductivity in the measured range is related to electrochemical reactions at the interface between the agar mixture and electrodes which cause parasitic contact impedance [20]. The influence of contact impedance declines with frequency and grows with NaCl doping. From the obtained results, it is observed that such a phenomenon can be neglected in all mixtures for frequency values above 1 kHz. In particular, note that the electrical conductivity and relative permittivity values for mixture no. 3 at 1 kHz are 0.325 S/m and $1.35 \cdot 10^5$, respectively.

The electrical conductivity and relative permittivity of mixtures no. 1, 3 and 5 were also investigated from the viewpoint of the influence of the voltage applied to the sample.

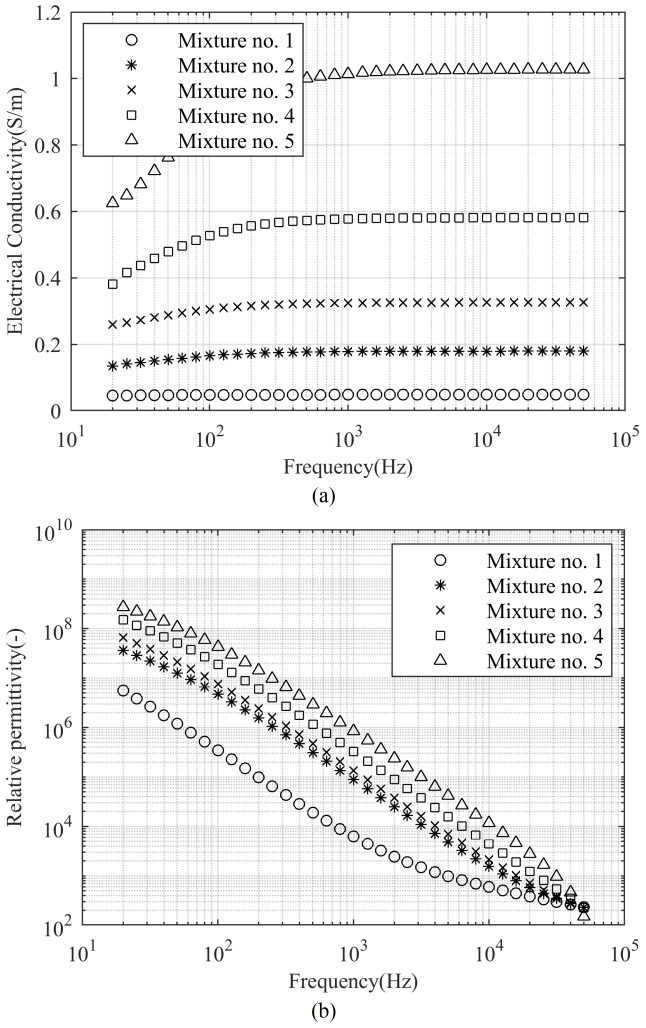

FIGURE 2. Electrical conductivity (a) and relative permittivity (b) of mixtures summarized in Table 1.

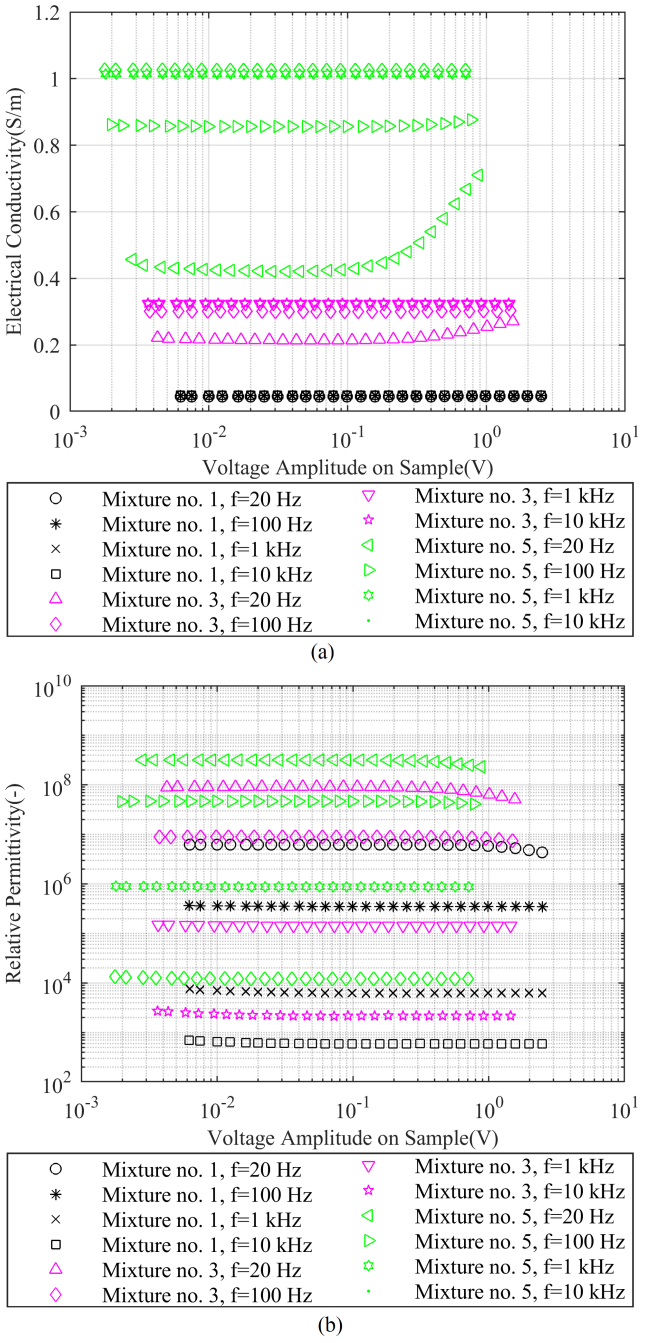

FIGURE 3. Applied-voltage dependence of electrical conductivity (a) and relative permittivity (b) for mixtures no. 1, 3 and no. 5.

We changed the voltage level of the impedance meter oscillator from 5 mV to 2 V, and we carried out the measurement at frequencies of 20 Hz, 100 Hz, 1 kHz and 10 kHz. The results are depicted in Fig. 3. We can see that the conductivity measured for mixture no. 1 is constant for all frequencies. However, the conductivity of mixtures no. 3 and no. 5 at the frequencies 20 Hz and 100 Hz depends on the applied voltage and so violates linearity. The conductivity for the frequencies 1 kHz and 10 kHz is constant. In the case of relative permittivity, we can see small voltage dependences mainly for 20 Hz and 100 Hz.

To compare the results of electrical conductivity with model (1) [20], and (2) [5], the following linear regression model from the measured data collected at 50 kHz was obtained

$$\sigma = 178 \cdot c + 0.066. \tag{5}$$

The graphical comparison of all three models is depicted in Fig. 4. Obviously, our model fits satisfactorily with the model defined by (2) [5], which indicates the purity of our constituents was similar to those used in [5].

As mentioned, the agar based phantoms degrade over time due to the loss of water and possible growth of fungi. To minimize water evaporation, agar based phantoms should be wrapped in a plastic film or located in a hermetic sealing box. A study of storage effects on degradation of water-based phantoms [22] indicated that a plastic film and a hermetically sealed box can extend their lifetime by about a month and a year, respectively.

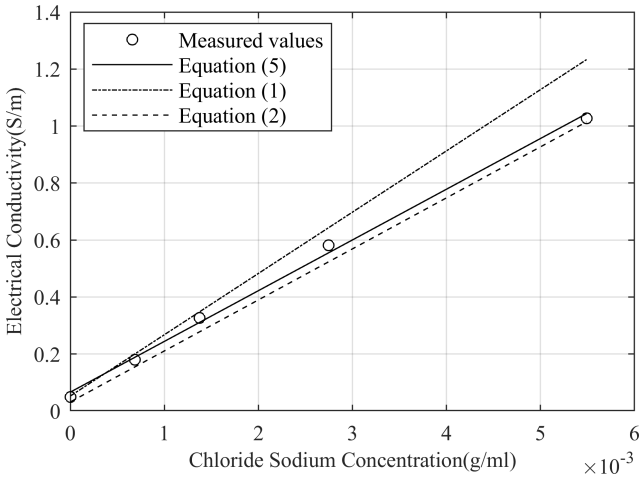

FIGURE 4. Graphical comparison of all models for prediction of electric conductivity of agar based mixtures.

Since the investigated agar mixtures do not contain any preservatives, agar based phantoms should be stored in a fridge [23] to avoid possible fungi growth.

Note that to have good reproducibility of an agar based mixture, it is necessary to keep the same fabrication process.

B. EXPLOITATION OF AGAR BASED MIXTURE AT HIGH FREQUENCIES

In the previous part, we observed that the voltage dependency of the measured properties allows us to exploit the agar based mixtures at higher frequencies only. So let's now concentrate whether it will be feasible to exploit the mixture at high frequencies (above 1 kHz).

Since the most important part of the EEG spectrum is up to lower hundreds of Hz, the forward problem is usually modeled quasi-statically by Poisson's differential equation [1]

$$\nabla \cdot (\sigma \nabla V) = -I. \tag{6}$$

Here, V is the electric potential, and I is the source current. Equation (6) considers only the conductive current whereas the displacement one is neglected. Thus, it is essential to validate whether the phantom operating at 1 kHz can still simulate the brain signals well.

In order to describe an electromagnetic (EM) problem completely, the full-wave equation which considers both currents should be used [24]

$$\nabla^2 \boldsymbol{A} + \omega (\omega\varepsilon - j\sigma) \boldsymbol{A} = -\mu \boldsymbol{J}. \tag{7}$$

Here, μ and ε are permeability and permittivity of the surrounding environment, ω is the angular frequency, $\boldsymbol{A}$ is the unknown vector potential, and $\boldsymbol{J}$ is the source current density.

Comparison of both equations (6) and (7) leads to the following requirements on the agar mixture for exploitation at high frequencies:

1. The mixture has to have permeability of a vacuum.
2. The fabricated phantom based on the agar mixture has to be much smaller than the wavelength in the medium of the agar mixture.
3. To neglect the displacement current, the conductivity of agar mixture σ has to be much higher than the permittivity of the mixture multiplied by angular frequency.

The first requirement is satisfied since the constituents of the agar mixture have the desired permeability. The second requirement is met considering the computed wavelength in the mixture depicted in Fig. 5. The last requirement is also met since the product of the angular frequency and the permittivity is much lower than the conductivity of mixtures (compare Fig. 6 and Fig. 2) as verified for all 5 mixtures.

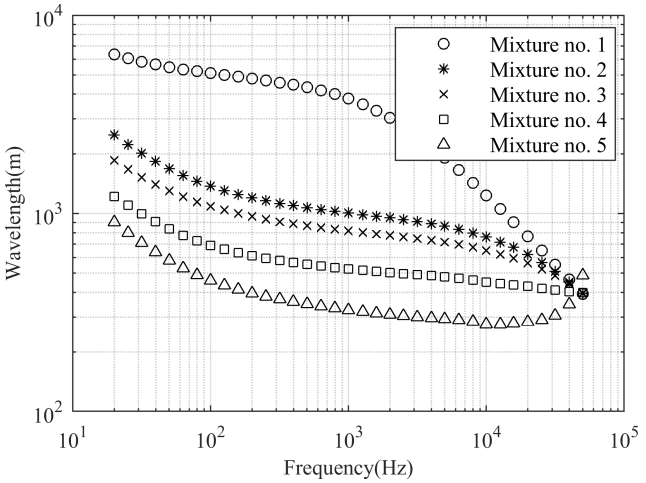

FIGURE 5. Wavelength in agar mixtures.

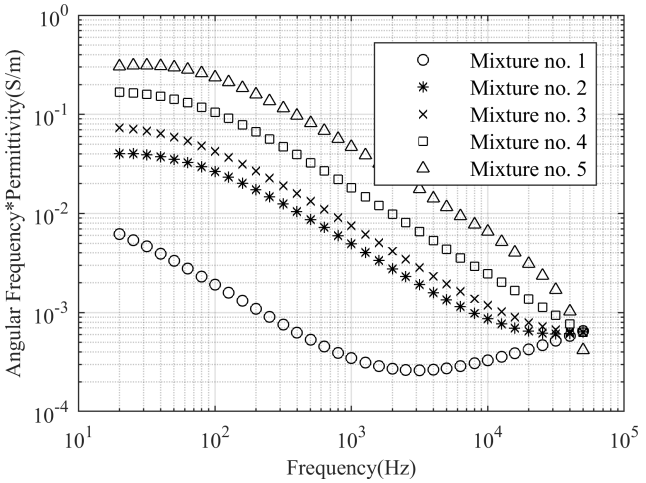

FIGURE 6. Dependence of angular frequency multiplied by permittivity of mixtures on frequency.

Since all requirements are met, the phantom can be used from 1 kHz up.

III. MODELING NEURAL ACTIVITY OF THE BRAIN

The neural activity of the brain can be modeled by electric dipoles which are realized by thin coaxial cables. The first

arm of the dipole is created by a small cylinder which is pressed on the inner conductor of the coaxial cable. The second arm of the dipole is created by the bent outer conductor of the coaxial cable. The length of each dipole arm is 2 mm approximately, and the gap between the arms is 0.5 mm approximately. The diameter of the fabricated dipole is 1.4 mm. For monitoring the surface electric potential, small conventional pins are used.

Both the electric dipoles and the electrodes were platinum coated (Fig. 7).

(a) (b)

FIGURE 7. Used electric dipoles (a) for modeling neural activity and electrode pins (b) for monitoring surface electric potential.

IV. RAT HEAD PHANTOM FABRICATION

A. SKULL

To fabricate a rat head phantom of realistic shape, the skull has to be created. The skull is the shell for the final agar mixture. Further, the skull carries excitation dipoles and electrodes to approximate and monitor the behavior of active neurons.

To create a realistic model of a skull, a computed tomography (CT) scan of the rat skull [25], [26] was exploited and slightly modified. Small holes in the skull were removed. A low-profile brick was added to the model to have a stable base for the excitation dipoles and the skull was cut into two parts. Both parts were scaled up by 1.8 and printed by a 3D printer based on stereolithography (SLA) technology. For printing, we used a Formlab standard resin [27].

B. PHANTOM FABRICATION

To fabricate the phantom, at first 14 electrodes were placed on the upper part of the scaled up skull (Fig. 8(a)). Their organization corresponds with the scheme for the rat EEG measurement described in [16]. Note that the electrode G1 was added to the interparietal bone since the electrical voltage was measured with respect to that electrode. Furthermore, this configuration was originally optimized to avoid artifacts during signal acquisition in freely moving animals. We considered the original measurement setup.

At the desired position, a small hole was drilled and an electrode in the hole was fixed with a hot melt glue gun. To measure electric potential on the brain surface, the tips of all the electrodes were aligned with the inner surface of the skull.

Secondly, six excitation electric dipoles were fixed to the lower part of the skull with a hot melt glue gun. The organization of the dipoles on the base is depicted in Fig. 8(b).

Thirdly, both parts of the skull were fixed together with a hot melt glue gun. The final skull with excitation dipoles and electrodes is depicted in Fig. 8(c).

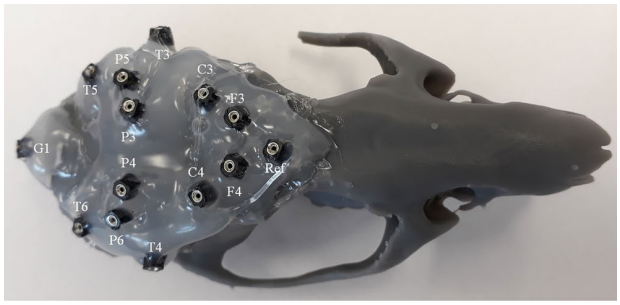

(a)

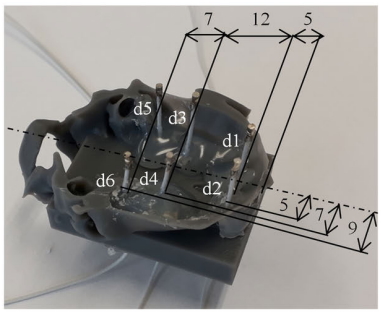

(b)

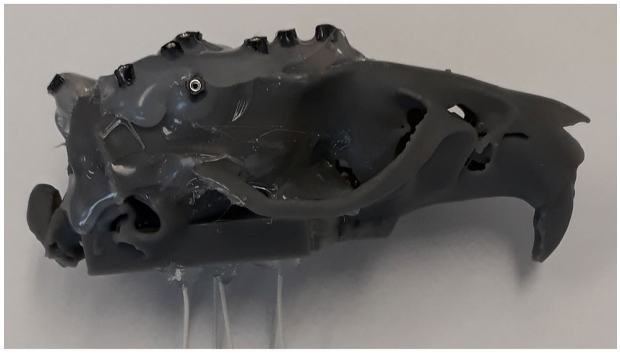

(c)

FIGURE 8. Upper part of skull with electrodes (a), lower part of skull with excitation dipoles (b) and complete skull (c).

Finally, the agar mixture mimicking the gray matter was prepared carefully according to the procedure described in Section 2.A and poured into the skull. After cooling the mixture to room temperature, the phantom was tested.

V. RAT HEAD PHANTOM TESTING

To test the fabricated phantom, the excitation dipoles were gradually connected to the generator IQ SIGLENT SDG6022X which provided a harmonic signal of frequency 1 kHz. The electrodes of the phantom were connected to BioSDA09, a standard 32-channel digital EEG amplifier (MI Ltd., Prague, Czech Republic), via a 14-lead cable (Data Sciences International, St. Paul, Minnesota, United States) connected to the electrodes by a dual-row IO socket connector. Sampling frequency was set to 5 kHz. The measurement workplace is depicted in Fig. 9.

The following testing procedures were carried out:

1. Each excitation dipole was gradually connected to the generator whose amplitude was set to 20 mV.

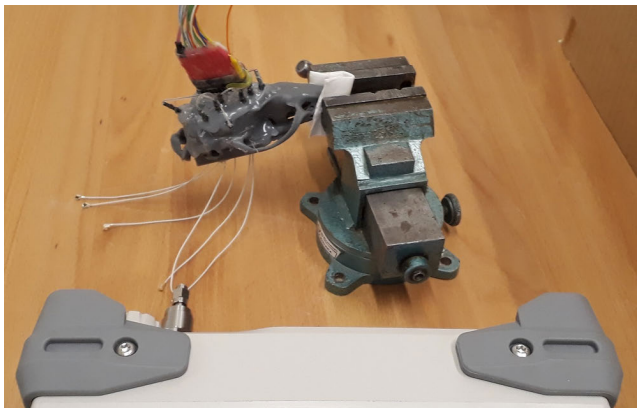

FIGURE 9. Testing of fabricated rat head phantom.

2. The dipole d1 was excited with different amplitude changing from 6 to 200 mV.

For both procedures, a voltage between each sensing electrode and the electrode G1 (Fig. 8(a)) was measured. After that, within the frame of postprocessing, the recorded voltage was recalculated with respect to the electrode Ref and the Fourier transformation was applied. The resultant measured electrode voltages are twice the magnitudes of the Fourier series coefficient corresponding to 1 kHz. Note that for a source localization procedure, the complex Fourier coefficients have to be considered.

The results of testing procedure 1 are presented in Fig. 10. To test the feasibility of the fabricated phantom for source localization studies, the following data analysis pipeline was implemented.

A homogeneous brain volume conduction model was calculated utilizing the finite element method implemented in the SimBio software [28] interfaced with the FieldTrip toolbox [29] in MATLAB. The forward model geometry was defined based on the same CT scan of the rat skull as it was used for the phantom fabrication. The brain volume was discretized onto 450 thousand tetrahedrons. The quasi-static formulation of the forward problem was considered in this case. For a realistic brain shape and a finite number of electrodes, the forward problem [1] can take the following form

$$\boldsymbol{X} = \boldsymbol{K}\boldsymbol{Y} + \boldsymbol{e}, \tag{8}$$

where $\boldsymbol{X}$ is a column vector (number of electrodes) of data measurements, $\boldsymbol{K}$ (number of electrodes x number of dipoles) is a so-called lead field matrix, $\boldsymbol{Y}$ is a column vector (number of dipoles) representing current dipole moments and $\boldsymbol{e}$ is a column vector (number of electrodes) denoting an additive noise of the model.

A regular grid of candidate dipoles was generated inside the brain volume. Dipole spacing was set to 2 mm which resulted in 2346 dipoles inside the brain volume.

Electrodes were co-registered with the discretized brain geometry, projected onto the brain surface, and assigned to the closest node of the computational mesh.

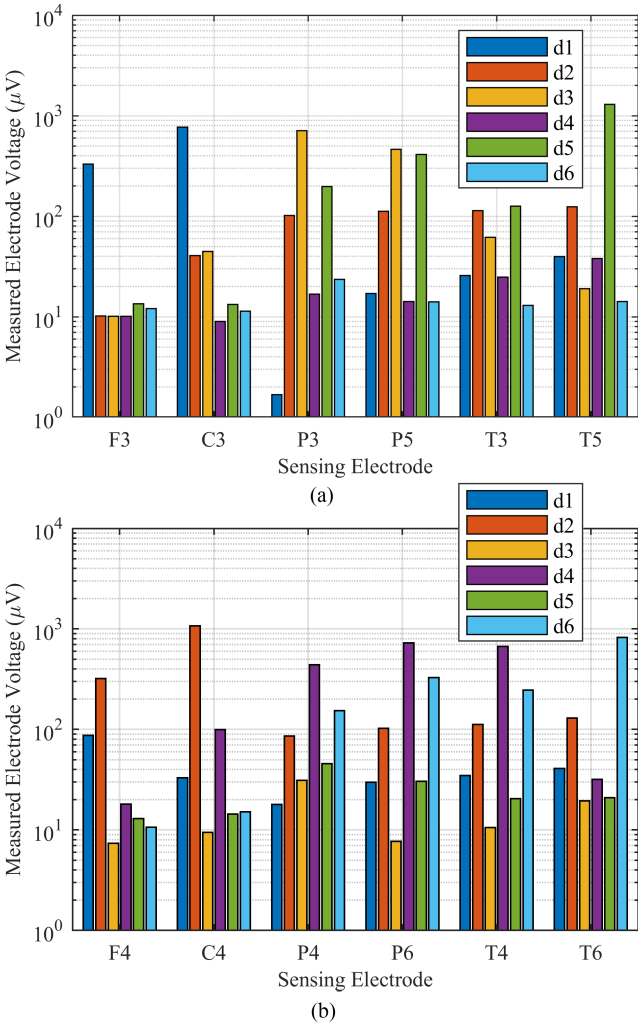

FIGURE 10. Measured electrode voltages for gradual excitation of dipole d1-d6: (a) left side sensing electrodes F3, C3, P3, P5, T3, T5, (b) right side sensing electrodes F4, C4, P4, P6, T4, T6.

Finally, the source localization technique called eLORETA [30] was applied to the data. This inverse solver belongs to the family of weighted minimum norm solutions and can be expressed as follows [30]

$$\boldsymbol{Y}_{p_{eLOR}} = \boldsymbol{W}_p^{-1}\boldsymbol{K}_p^T\left(\boldsymbol{K}_P\boldsymbol{W}_p^{-1}\boldsymbol{K}_p^T + \gamma\boldsymbol{I}\right)^{-1}\boldsymbol{X}, \tag{9}$$

where p denotes a dipole index in the brain volume, T transpose, $\boldsymbol{I}$ identity matrix, γ is a regularization parameter, and $\boldsymbol{W}$ represents the weighting matrix which solution can be found numerically by solving the equation [30]

$$\boldsymbol{W}_p = \left[\boldsymbol{K}_p^T\left(\boldsymbol{K}\boldsymbol{W}^{-1}\boldsymbol{K}^T - \gamma\boldsymbol{I}\right)^{-1}\boldsymbol{K}_p\right]^{-\frac{1}{2}}. \tag{10}$$

All models were implemented in the FieldTrip software [29] in MATLAB.

The true dipole positions were obtained by the computed tomography (CT) scanning. The CT scan was co-registered with the dipole grid using ITK-SNAP software [31] and each

source estimation was interpolated and printed over the CT scan volume (Fig. 11).

Recorded data from all six dipole excitations were subsequently localized in the brain volume. The localization technique resulted in a smoothly distributed source power around the original dipole positions (Fig. 11). Distances between the globally maximal power locations and true dipole positions were considered as quantitative measure of localization accuracy.

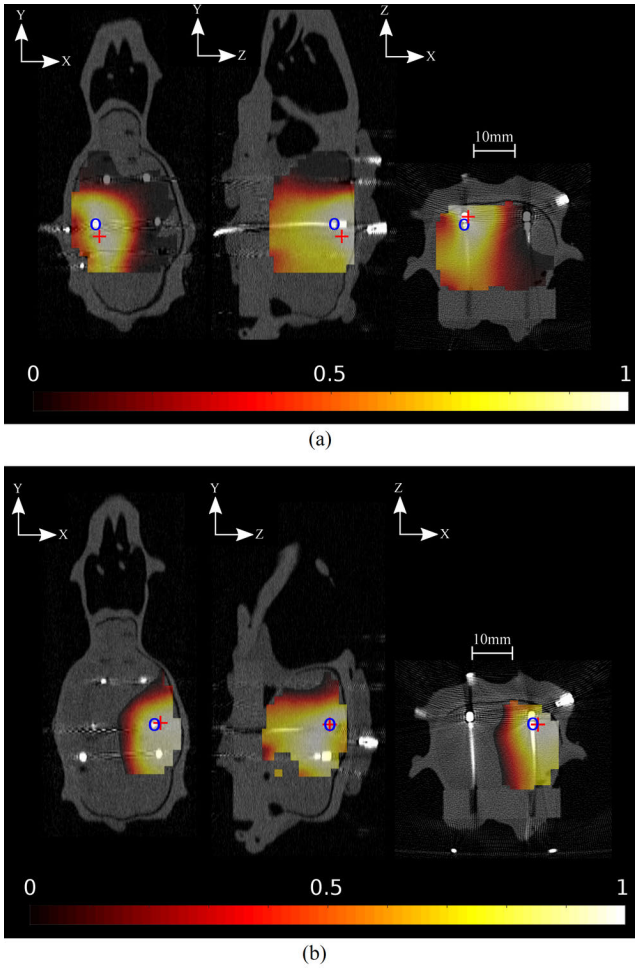

FIGURE 11. Normalized source distributions estimated for d3 (a) and d4 (b) excitations corresponding to the worst and the best accuracy respectively. The normalized estimated source power (hot colormap) was interpolated onto the CT scan (gray scale), reference dipole positions are marked with a circle, and global maxima of source distributions are marked with a cross. Power values were normalized with respect to their maximum value in each instance d3 and d4 excitation, thus the source distribution is presented by a unitless quantity here.

Error of the inverse procedure summarized in Table 2 was calculated in the following way:

- Each reference dipole was considered to be a point source with specific coordinates X, Y, and Z.
- The global maximum of each estimated source distribution was found and this maximum was treated as point source estimation in X, Y, and Z coordinates.

TABLE 2. Error of source localization technique in case of single dipole excitation.

Error	Dipole d1 (mm)	Dipole d2 (mm)	Dipole d3 (mm)	Dipole d4 (mm)	Dipole d5 (mm)	Dipole d6 (mm)
Euclidean	1.0	1.4	3.7	1.0	1.4	1.0
X	0.0	0.0	1.0	1.0	-1.0	0.0
Y	0.0	-1.0	-3.0	0.0	1.0	0.0
Z	1.0	1.0	2.0	0.0	0.0	-1.0

- The distance of each global maximum from its reference dipole position was calculated in all directions separately to address error bias in any specific direction
- Finally, the Euclidean distances between reference dipole positions and estimated global maxima were calculated.

Fig. 11 depicts the source distributions for the best and the worst accurate estimations. Here, the precision of the estimates can be observed.

As it was reported in [9], the estimated sources were systematically attracted to the electrodes towards the phantom surface. In our case, this would correspond to a systematic shift of the locations in positive direction of the Z axis. However, due to the realistic geometry we can't observe this phenomenon clearly. In our case, the estimated source locations were slightly shifted rather towards the closest electrodes with respect to the real dipole positions. We understand this as the same phenomena as reported in [9]. However, our results further validated that the depth bias was sufficiently weighted and compensated by the eLORETA approach and indicate that eLORETA can be used in future research in source localization in rats.

Based on the known dipole positions we were able to compare various regularization settings. Inverse models based on different values of the regularization parameter exhibited negligible differences by observing the estimated source distributions. However, quantitative comparison showed changes in the range of millimeters. Thus, it was valuable to implement a cross-validation algorithm for estimating an optimal value of the regularization parameter. The lowest localization errors were obtained when the inverse model minimized the leave one out cross validation criterion.

Smoothness of the estimated source distributions is similar for all dipole excitations. Fig. 11 depicts the source distributions for the most and the least accurate estimates. This uncertainty is intrinsically involved in the whole system: measured data, forward model errors, and electrode distribution. Here, the sparsity of the electrodes is considered as the main factor reducing precision of estimation. In order to achieve more accurate source distributions, more sensing electrodes are needed as it was described for the case of a human [32]. However, a number of electrodes has to be carefully chosen with respect to invasiveness of surgery, physical dimension of

the electrodes, and effectiveness after regularization. We estimated that approximately 25 electrodes is the limit of the current cortical EEG system.

All EEG measurements were performed in the same day as the phantom was fabricated. However, there was approximately one month prolongation when we had to wait for free slots in the CT scanner. A slim contrasting layer between the agar brain and scull can be observed in the CT scan in Fig. 11. This was due to prolongation of the CT scanning procedure and slight water evaporation of the agar mixture although the phantom was wrapped in a plastic foil and located in a fridge to minimize it.

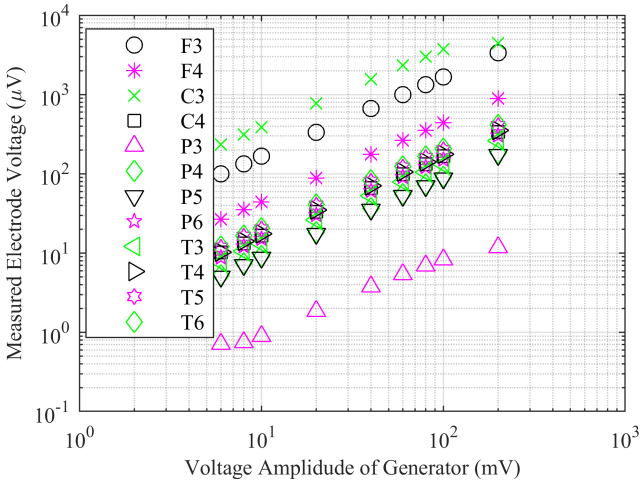

FIGURE 12. Measured electrode voltages at rat head phantom for excitation dipole d1.

The results of testing procedure 2 are depicted in Fig. 12 where we can see the dependencies of the measured electrode voltages on the voltage amplitude of the generator. Evidently, the excitation amplitudes for the testing procedure 1 were correctly chosen since the phantom operates in a linear regime. Note that electrode C3 is located directly above the excitation dipole d1, so the measured electrode voltage reaches the highest values. Further, we can also observe for the C3 response the saturation of our amplifier.

VI. CONCLUSIONS

In this paper we introduced a low-cost rat head phantom which can be fabricated with currently available conventional techniques. Its life span is relatively short as for all water/agar-based phantoms. To prolong its life span, the phantom should be wrapped in a plastic film or a hermetically sealed box and stored in a fridge.

We used the fabricated phantom to test the currently available cortical electrode implant. Precision of localization of individual dipoles was comparable with the mean inter-electrode distance which is considered to be a supporting result for further development of the implant towards reliable source localization in rats.

Inverse models based on different values of the regularization parameter exhibited error differences within a range of millimeters. We found that localization errors could be significantly reduced by using the regularization parameter obtained through cross-validation.

An advantage of the present phantom is its realistic geometry which allowed us to simulate a realistic distribution of electrodes and test the depth bias in source localization. These results could not have been obtained with the flat design of previously published electrode systems. We also tested the eLORETA approach in compensating the depth bias and thanks to promising results we suggest to use eLORETA for future research in source localization in rats.

The proposed technique is versatile and allows further development of the cortical electrode system or its application in other scenarios. For example, the phantom allows using a combination of depth and cortical electrodes to simulate signals recorded during localization of epileptic seizures. Compared to validation approaches on living animals, this phantom based approach allows better controlled experimental conditions and it is appealing from an ethical point of view.

Regarding the results obtained by source localization techniques, we can conclude that future implants should utilize more electrodes to decrease the bias of the source positions and increase precision. However, the number of electrodes used in the future has to be carefully chosen with respect to invasiveness of surgery and the physical dimension of the electrodes. Moreover, increasing the number of electrodes should be addressed by appropriate statistical criterion to take into account noise perturbation and regularization of the inverse solution.

REFERENCES

[1] H. Hallez, B. Vanrumste, R. Grech, J. Muscat, W. De Clercq, A. Vergult, Y. D'Asseler, K. P. Camilleri, S. G. Fabri, S. Van Huffel, and I. Lemahieu, "Review on solving the forward problem in EEG source analysis," *J. NeuroEng. Rehabil.*, vol. 4, no. 1, p. 46, Nov. 2007.

[2] D. L. Collins, A. P. Zijdenbos, V. Kollokian, J. G. Sled, N. J. Kabani, C. J. Holmes, and A. C. Evans, "Design and construction of a realistic digital brain phantom," *IEEE Trans. Med. Imag.*, vol. 17, no. 3, pp. 463–468, Jun. 1998.

[3] C. H. Wolters, A. Anwander, X. Tricoche, D. Weinstein, M. A. Koch, and R. S. MacLeod, "Influence of tissue conductivity anisotropy on EEG/MEG field and return current computation in a realistic head model: Asimulation and visualization study using high-resolution finite element modeling," *NeuroImage*, vol. 30, no. 3, pp. 813–826, 2006.

[4] F. J. Beekman, B. Vastenhouw, G. van der Wilt, M. Vervloet, R. Visscher, J. Booij, M. Gerrits, C. Ji, R. Ramakers, and F. van der Have, "3-D rat brain phantom for high-resolution molecular imaging," *Proc. IEEE*, vol. 97, no. 12, pp. 1997–2005, Dec. 2009.

[5] D. Kim, J. Jeong, S. Jeong, S. Kim, S. C. Jun, and E. Chung, "Validation of computational studies for electrical brain stimulation with phantom head experiments," *Brain Stimulation*, vol. 8, no. 5, pp. 914–925, Sep. 2015.

[6] R. J. Cooper, R. Eames, J. Brunker, L. C. Enfield, A. P. Gibson, and J. C. Hebden, "A tissue equivalent phantom for simultaneous near-infrared optical tomography and EEG," *Biomed. Opt. Express*, vol. 1, no. 2, pp. 425–430, 2010.

[7] R. M. Leahy, J. C. Mosher, M. E. Spencer, M. X. Huang, and J. D. Lewine, "A study of dipole localization accuracy forMEG and EEG using a human skull phantom," *Electroencephalogr. Clin. Neurophysiol.*, vol. 107, no. 2, pp. 159–173, Apr. 1998.

[8] T. J. Collier, D. B. Kynor, J. Bieszczad, W. E. Audette, E. J. Kobylarz, and S. G. Diamond, "Creation of a human head phantom for testing of electroencephalography equipment and techniques," *IEEE Trans. Biomed. Eng.*, vol. 59, no. 9, pp. 2628–2634, Sep. 2012.

[9] H. Yang and H. Jiang, "Design and evaluation of a miniature probe integrating diffuse optical tomography and electroencephalographic source localization," *Appl. Opt.*, vol. 52, no. 20, pp. 5036–5041, Jul. 2013.
[10] J.-B. Li, M.-X. Tang, X.-Z. Dong, C. Tang, M. Dai, G. Liu, X.-T. Shi, B. Yang, C.-H. Xu, F. Fu, and F.-S. You, "A new head phantom with realistic shape and spatially varying skull resistivity distribution," *IEEE Trans. Biomed. Eng.*, vol. 61, no. 2, pp. 254–263, Feb. 2014.
[11] P. C. Hansen, *Discrete Inverse Problems*. Philadelphia, PA, USA: Society for Industrial and Applied Mathematics, 2010.
[12] J. Bae, A. Deshmukh, Y. Song, and J. Riera, "Brain source imaging in preclinical rat models of focal epilepsy using high-resolution EEG recordings," *J. Visualized Exp.*, vol. 100, Jun. 2015, Art. no. e52700.
[13] H. Yang, T. Zhang, J. Zhou, P. R. Carney, and H. Jiang, "*In vivo* imaging of epileptic foci in rats using a miniature probe integrating diffuse optical tomography and electroencephalographic source localization," *Epilepsia*, vol. 56, no. 1, pp. 94–100, Jan. 2015.
[14] P. A. Valdés-Hernández, J. Bae, Y. Song, A. Sumiyoshi, E. Aubert-Vázquez, and J. J. Riera, "Validating non-invasive EEG source imaging using optimal electrode configurations on a representative rat head model," *Brain Topography*, vol. 32, no. 4, pp. 599–624, Jul. 2019.
[15] C. Lee, R. Oostenveld, S. H. Lee, L. H. Kim, H. Sung, and J. H. Choi, "Dipole source localization of mouse electroencephalogram using the fieldtrip toolbox," *PLoS ONE*, vol. 8, no. 11, Nov. 2013, Art. no. e79442.
[16] T. Páleníček, M. Fujáková, M. Brunovský, M. Balíková, J. Horáček, I. Gorman, F. Tylšf, B. Tišlerová, P. Šoš, V. Bubeníková-Valešová, C. Höschl, and V. Krajča, "Electroencephalographic spectral and coherence analysis of ketamine in rats: Correlation with behavioral effects and pharmacokinetics," *Neuropsychobiology*, vol. 63, no. 4, pp. 202–218, 2011.
[17] C. Gabriel, A. Peyman, and E. H. Grant, "Electrical conductivity of tissue at frequencies below 1 MHz," *Phys. Med. Biol.*, vol. 54, no. 16, pp. 4863–4878, Aug. 2009.
[18] S. Gabriel, R. W. Lau, and C. Gabriel, "The dielectric properties of biological tissues: III. Parametric models for the dielectric spectrum of tissues," *Phys. Med. Biol.*, vol. 41, no. 11, pp. 2271–2293, Nov. 1996.
[19] T. Goto, R. Hatanaka, T. Ogawa, A. Sumiyoshi, J. Riera, and R. Kawashima, "An evaluation of the conductivity profile in the somatosensory barrel cortex of wistar rats," *J. Neurophysiol.*, vol. 104, no. 6, pp. 3388–3412, Dec. 2010.
[20] D. Bennett, "NaCl doping and the conductivity of agar phantoms," *Mater. Sci. Eng., C*, vol. 31, no. 2, pp. 494–498, Mar. 2011.
[21] L. Rusiniak, "Dielectric properties and structure of water at room temperature. New experimental data in 5 Hz-13 mhz frequency range," *Phys. Chem. Earth, A, Solid Earth Geodesy*, vol. 25, no. 2, pp. 201–207, Jan. 2000.
[22] C. Mendes, and C. Peixeiro, "Fabrication, measurement and time decay of the electromagnetic properties of semi-solid water-based phantoms," *Sensors*, vol. 19, no. 19, pp. 1–21, Oct. 2019.
[23] J. Lacik, V. Hebelka, J. Velim, Z. Raida, and J. Puskely, "Wideband skin-equivalent phantom for V- and W-Band," *IEEE Antennas Wireless Propag. Lett.*, vol. 15, pp. 211–213, 2016.
[24] C. A. Balanis, *Advanced Enegineering of Electromagnetics*. Hoboken, NJ, USA: Wiley, 1989, pp. 254–261.
[25] B. M. Pohl, F. Gasca, O. Christ, and U. G. Hofmann, "3D printers May reduce animal numbers to train neuroengineering procedures," in *Proc. 6th Int. IEEE/EMBS Conf. Neural Eng. (NER)*, Nov. 2013, pp. 887–890.
[26] M. Pohl, F. Gasca, O. Christ and U. G. Hofmann. (Aug. 21, 2013). *3D.Stl File of Rat Skull, Figshare*. [Online]. Available: https://doi.org/10.6084/m9.figshare.777745.v1
[27] 3Dwiser Ltd. *Prague, Czech Republic*. Accessed: Dec. 9, 2019. [Online]. Available: https://eshop.3dwiser.com/pryskyrice/formlabs-standard-resins/
[28] J. Vorwerk, R. Oostenveld, M. C. Piastra, L. Magyari, and C. H. Wolters, "The FieldTrip-SimBio pipeline for EEG forward solutions," *Biomed. Eng. OnLine*, vol. 17, no. 1, p. 37, Dec. 2018.
[29] R. Oostenveld, P. Fries, E. Maris, and J.-M. Schoffelen, "FieldTrip: Open source software for advanced analysis of MEG, EEG, and invasive electrophysiological data," *Comput. Intell. Neurosci.*, vol. 2011, pp. 1–9, Dec. 2011.
[30] R. D. Pascual-Marqui, "Discrete, 3D distributed, linear imaging methods of electric neuronal activity—Part 1: Exact, zero error localization," 2007, *arXiv:0710.3341*. [Online]. Available: http://arxiv.org/abs/0710.3341
[31] P. A. Yushkevich, J. Piven, H. C. Hazlett, R. G. Smith, S. Ho, J. C. Gee, and G. Gerig, "User-guided 3D active contour segmentation of anatomical structures: Significantly improved efficiency and reliability," *NeuroImage*, vol. 31, no. 3, pp. 1116–1128, Jul. 2006.
[32] J. Song, C. Davey, C. Poulsen, P. Luu, S. Turovets, E. Anderson, K. Li, and D. Tucker, "EEG source localization: Sensor density and head surface coverage," *J. Neurosci. Methods*, vol. 256, pp. 9–21, Dec. 2015.

JAROSLAV LACIK (Member, IEEE) received the M.Sc. and Ph.D. degrees from the Brno University of Technology, Brno, Czech Republic, in 2002 and 2007, respectively. He is currently an Associate Professor with the Brno University of Technology. His research interests are antennas, body-centric wireless communication, computational electromagnetics, and measurement.

VLASTIMIL KOUDELKA was born in Usti nad Labem, Czech Republic. He received the M.Sc. and Ph.D. degrees from the Brno University of Technology, in 2009 and 2014, respectively. He is currently a Junior Researcher with the National Institute of Mental Health, Klecany. He is interested in the analysis and integration of neuroimaging data, machine learning, and signal synchronization in multimodal signal acquisition.

DAVID KURATKO received the M.Sc. degree from the Department of Radio Electronics, Faculty of Electrical Engineering and Communication (FEEC), Brno University of Technology (BUT), in 2018, where he is currently pursuing the Ph.D. degree with the Department of Radio Electronics, FEEC. His research interest is focused on the rat's head forward modeling.

ZBYNEK RAIDA (Senior Member, IEEE) received the M.Sc. and Ph.D. degrees from the Brno University of Technology (BUT), in 1991 and 1994, respectively. He is currently a Professor with the BUT. His research interests include applied electromagnetics, computational electromagnetics, and the exploitation of artificial intelligence techniques for electromagnetic design.

DANIEL KRZYSZTOF WÓJCIK received the M.Sc. and Ph.D. degrees from the Department of Physics, University of Warsaw, in 1996 and 2000, respectively, and the Habilitation degree from the Institute of Physics, Polish Academy of Sciences (PAS), in 2008. He was a Research Assistant with the Center for Theoretical Physics, PAS, from 1996 to 2000. He worked at the Institute for Physical Science and Technology, University of Maryland, from 2000 to 2002, and the School of Physics, from 2002 to 2003, on the deterministic models of quantum walks. In 2003, he joined the Nencki Institute of Experimental Biology, PAS, where he is currently a Professor and the Head of the Laboratory of Neuroinformatics. Since 2019, he has been running the Neuro Group within Bioinspired Artificial Neural Networks Consortium, Jagiellonian University. He is an Adjunct Research Professor with the Brno University of Technology.

TOMAS MIKULASEK received the M.Sc. and Ph.D. degrees in electrical engineering and communication from the Brno University of Technology, Brno, Czech Republic, in 2009 and 2013, respectively. He is currently a Researcher with the Department of Radio Electronics, Faculty of Electrical Engineering and Communication, Brno University of Technology. His research interests include microwave antennas and components based on substrate integrated waveguide.

JIRI VANEK received the Ph.D. degree from the Brno University of Technology, Brno, Czech Republic, in 2004. He is currently an Associate Professor with the Department of Electrical and Electronics Technology, Faculty of Electrical Engineering and Communication, Brno University of Technology. His research interests are in the diagnostics methods of materials properties, technology and design, photovoltaics, and other renewable sources of energies.

STANISLAV JIRICEK received the M.Sc. degree from the Faculty of Biomedical Engineering, Czech Technical University in Prague, in 2019, where he is currently pursuing the Ph.D. degree in bioengineering with the Faculty of Electrical Engineering, Department of Cybernetics. He is also a part of the Complex Networks and Brain Dynamics Group, Department of Complex Systems, Institute of Computer Science, and also the Applied Neuroscience and Neuroimaging Research Programme of the National Institute of Mental Health.

CESTMIR VEJMOLA received the M.Sc. degree from the Faculty of Science, Charles University in Prague. He is currently pursuing the master's degree with the National Institute of Mental Health, Klecany. He is interested in translational neuroscience, the animal models of mental diseases, electrophysiology, and bioelectronics.